Coalescence of nonreciprocal exceptional points in magnetized $\mathcal{PT}$-symmetric systems

Jin Wang,[1,2,*] Hui Yuan Dong,[3] Qian Yi Shi,[1] Wenyan Wang,[2] and Kin Hung Fung[2,†]
[1]*School of Physics, Southeast University, Nanjing 211189, China*
[2]*Department of Applied Physics, The Hong Kong Polytechnic University, Hong Kong, China*
[3]*School of Science, Nanjing University of Posts and Telecommunications, Nanjing 210003, China*

(Received 4 October 2017; revised manuscript received 29 December 2017; published 22 January 2018)

We study the Lorentz nonreciprocal transmission and nonreciprocal complex band structures supported in a $\mathcal{PT}$-symmetric waveguide sandwiched by magnetized layers. We found that, near the emergency and coalescence of exceptional points, nonreciprocal transmission can be significantly enhanced by the non-Hermitian properties. With the help of gain-loss balance, one-way light transmission could be achieved even in the presence of a weak magnetic field. The results may offer us insight into the interplay between Lorentz nonreciprocity and non-Hermiticity.

DOI: 10.1103/PhysRevB.97.014428

I. INTRODUCTION

In the past decade, considerable research attention has been directed toward a kind of non-Hermitian Hamiltonian respecting parity-time ($\mathcal{PT}$) symmetry, for the purpose of studying non-Hermitian physics. By definition, a Hamiltonian $\hat{H}$ is considered to be $\mathcal{PT}$ symmetric, $[\hat{H}, \hat{P}\hat{T}] = 0$, implying that it shares common eigenfunctions with $\hat{P}\hat{T}$ operators [1–3]. Here, the action of parity operator $\hat{P}$ is defined by the transformation $\hat{p} \to -\hat{p}$, $\hat{x} \to -\hat{x}$ while the time operator $\hat{T}$ by $\hat{p} \to -\hat{p}$, $\hat{x} \to \hat{x}$ and $i \to -i$, where $\hat{p}$ and $\hat{x}$ are the momentum and the position operators, respectively. In this case, a necessary condition for a Hamiltonian to be $\mathcal{PT}$ symmetric is that the potential function should obey $V(x) = V^*(-x)$ with balanced gain and loss. However, such requirement with complex potentials is difficult to implement in quantum-mechanical systems. In optics, owing to the formal equivalence of the Schrödinger equation with the Helmholtz equation in the paraxial approximation, $\mathcal{PT}$-symmetric Hamiltonians could be easily realized by the introduction of the system with $\mathcal{PT}$-symmetric refractive index profile, $n(x) = n^*(-x)$ [4].

Following the pioneering work of Bender and co-workers [1,2], a series of studies have shown that under certain conditions, $\mathcal{PT}$-symmetric Hamiltonians can exhibit entirely real eigenvalue spectra, which is similar to that of Hermitian Hamiltonians. Another intriguing characteristic associated with this class of Hamiltonians is the possibility of an abrupt phase transition behavior if the parameter controlling the degree of non-Hermiticity exceeds a critical value—also called the exceptional point (EP) [1]. Because the $\mathcal{PT}$ operator is antilinear, the eigenstates of the Hamiltonian may or may not be eigenstates of the $\mathcal{PT}$ operator [5]. When the non-Hermitian parameter goes beyond the EP, a spontaneous $\mathcal{PT}$-symmetry breaking will occur, and the eigenfunctions of the Hamiltonian cease to be eigenfunctions of the $\mathcal{PT}$ operator. As a consequence, at the EP, the energy spectra start to change from entirely real to partially or completely complex, and thereby the system undergoes the phase transition from $\mathcal{PT}$-symmetric phase to $\mathcal{PT}$-broken phase [6]. Meanwhile, a great deal of studies have shown that the existence of EPs could lead to a great variety of counterintuitive phenomena, such as double refraction [3], loss-induced transparency [5], power oscillations [7], unidirectional transmission or reflection [8–13], laser-absorber modes [14,15], enhanced spontaneous emission [16], and enhanced nanoparticle sensing [17].

Recently, more complex phenomena involved in the occurrence and evolution of EPs have been theoretically proposed and experimentally observed in $\mathcal{PT}$-symmetric multistate systems [18–28]. For example, Alaeian and Dionne [18] demonstrated that in a five-layer plasmonic waveguide having $\mathcal{PT}$ symmetry, coalescence and evolution of EPs could be tuned to support positive or negative refractive indices by changing the coupling between the waveguide layers. Ding *et al.* [19] studied the coalescence of EPs in one-dimensional $\mathcal{PT}$-symmetric photonic crystals. One type is the occurrence of a ring of EPs, leading to the formation of an island of $\mathcal{PT}$-broken phase, and thereby the restoration behavior of $\mathcal{PT}$ symmetry. Another type is involved in the coalescence of EPs to form high-order singularity. The ring of EPs near a Dirac-like cone was also observed experimentally by Zhen *et al.* [20] in a two-dimensional photonic crystal slab. Richer physical behaviors such as phase space with distinct topological properties could be present in a four-state acoustic system [21]. Given the abrupt change of system phase near an EP, one may tune the properties of a system flexibly by a small variation of certain external parameters [22–25].

Previous studies on the evolution process of EPs and its associated phenomena are mostly focused on nonmagnetic systems. Many have studied the so-called "unidirectional" or "one-way" reflectance in $\mathcal{PT}$-symmetric systems, which is still reciprocal in terms of transmittance due to Lorentz reciprocity [9,11–13]. In this work, we demonstrate that a $\mathcal{PT}$-symmetric waveguide bounded by magneto-optical materials such as magnetized semiconductors (SCs), may show

*jinwang@seu.edu.cn
†kin-hung.fung@polyu.edu.hk

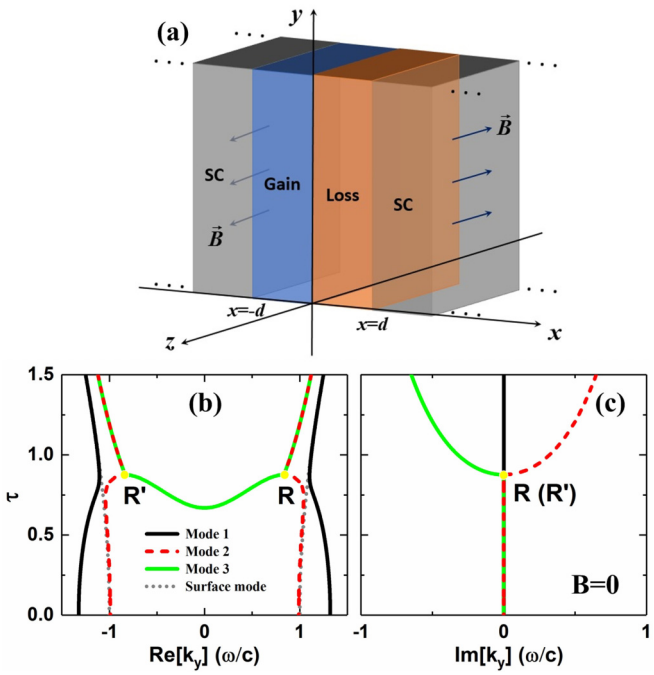

FIG. 1. (a) Schematic of $\mathcal{PT}$-symmetric plasmonic waveguides bounded by semi-infinite magnetized conductive layers. The blue arrows show the magnetization of the magnetic layers. (b) and (c) Amplitude of loss/gain τ versus real and imaginary parts of the propagation constant k_y, when an external magnetic field is absent ($B = 0$). Three guided modes (modes 1, 2, and 3) are shown by solid black), dashed red, and solid green lines, respectively. For comparison, the surface mode at the interface between semi-infinite lossy and gain materials is also shown by dotted gray lines. Possible EPs due to the coalescence of modes 2 and 3 are marked with R and R', respectively.

remarkable Lorentz nonreciprocity near the emergence or coalescence of EPs. Moreover, when the magnetized layers become thin, one-way light propagation could be achieved even if the external magnetic field is weak (<0.01 T). Our result may give insight into the interplay between Lorentz nonreciprocity and non-Hermiticity, and provide a mechanism to attain strong nonreciprocity in the presence of a weak magnetic field.

II. MODEL AND METHODS

Let us begin with a planar $\mathcal{PT}$-symmetric plasmonic waveguide as schematically illustrated in Fig. 1. Two dielectric loss and gain layers with identical thickness d and balanced dielectric constant ϵ_L and ϵ_G, $\epsilon_L(x) = \epsilon_G^*(-x) = \epsilon + i\tau$, are adjoined with two semi-infinite magnetized semiconductors. The external static magnetic field is applied on the two SC slabs along opposite directions, i.e., z and $-z$ axis (as indicated by blue arrows), forming a Voigt configuration. The dielectric constants of these two SCs can be expressed by two tensors $\bar{\epsilon}_{(x<-d)}$ and $\bar{\epsilon}_{(x>d)}$:

$$\bar{\epsilon}_{(x<-d)} = \begin{pmatrix} \epsilon_1 & i\Delta_1 & 0 \\ -i\Delta_1 & \epsilon_1 & 0 \\ 0 & 0 & \epsilon_1 \end{pmatrix}, \quad \bar{\epsilon}_{(x>d)} = \begin{pmatrix} \epsilon_2 & i\Delta_2 & 0 \\ -i\Delta_2 & \epsilon_2 & 0 \\ 0 & 0 & \epsilon_2 \end{pmatrix}. \tag{1}$$

We take the following parameters for magnetized SCs [29,30], i.e., $\epsilon_1 = \epsilon_2 = \epsilon_\infty[1 - \omega_p^2(1 + i\alpha/\omega)/((\omega + i\alpha)^2 - \omega_c^2)]$, $\Delta_1 = -\Delta_2 = -\epsilon_\infty\omega_p^2\omega_c/[\omega((\omega + i\alpha)^2 - \omega_c^2)]$. Here ϵ_∞ is the high-frequency permittivity, ω_p is the plasma frequency of SCs, the collision frequency α characterizes loss strength in SCs, $\omega_c = eB/m^*$ is the cyclotron frequency, e is the electron charge, and m^* is the effective mass of electrons. The magnetization parameters are chosen such that the SC layers also fulfill $\mathcal{PT}$ symmetry $\bar{\epsilon}_{(x>0)} = \bar{\epsilon}^*_{(x<0)}$, which guarantees the formation of purely real guided modes seen below. It should be noted that we consider the propagation of a TM-polarized light beam (i.e., only E_x, E_y, and H_z components of the electric and magnetic field are nonzero) along the y direction and use the $e^{-i\omega t}$ time-dependent convention for oscillating fields. The electromagnetic fields in each layer can be written as follows:

For $-d < x < 0$,

$$H_z = [A\cos(k_{Gx}x) + B\sin(k_{Gx}x)]e^{ik_y y},$$
$$E_y = \frac{k_{Gx}}{i\omega\epsilon_G}[-A\sin(k_{Gx}x) + B\cos(k_{Gx}x)]e^{ik_y y}. \tag{2}$$

For $0 < x < d$,

$$H_z = [C\cos(k_{Lx}x) + D\sin(k_{Lx}x)]e^{ik_y y},$$
$$E_y = \frac{k_{Lx}}{i\omega\epsilon_L}[-C\sin(k_{Lx}x) + D\cos(k_{Lx}x)]e^{ik_y y}. \tag{3}$$

For $x < -d$,

$$H_z = Ee^{\beta(x+d)}e^{ik_y y},$$
$$E_y = \frac{k_y\Delta_1 + \beta\epsilon_1}{i\omega(\epsilon_1^2 - \Delta_1^2)}Ee^{\beta(x+d)}e^{ik_y y}. \tag{4}$$

For $x > d$,

$$H_z = Fe^{-\gamma(x-d)}e^{ik_y y},$$
$$E_y = \frac{k_y\Delta_2 - \gamma\epsilon_2}{i\omega(\epsilon_2^2 - \Delta_2^2)}Fe^{-\gamma(x-d)}e^{ik_y y}. \tag{5}$$

Here A, B, C, and D are the amplitudes of the electromagnetic fields, and k_y is the propagation constant of the waveguide. k_{Gx}, k_{Lx}, β, and γ are defined as $k_{Gx} = \sqrt{\epsilon_G\mu k_0^2 - k_y^2}$, $k_{Lx} = \sqrt{\epsilon_L\mu k_0^2 - k_y^2}$, and $\beta = \gamma = \sqrt{k_y^2 - \epsilon_f\mu k_0^2}$, where $\epsilon_f = (\epsilon_1^2 - \Delta_1^2)/\epsilon_1$ is the effective permittivity of magnetized SC. By considering the boundary conditions that the tangential field components H_z and E_y should be continuous across each interface, we have the following dispersion relation of the waveguide:

$$\left(\frac{k_{Gx}(\epsilon_1^2 - \Delta_1^2)}{\epsilon_G(\beta\epsilon_1 + k_y\Delta_1)} - \frac{\epsilon_G(\beta\epsilon_1 + k_y\Delta_1)}{k_{Gx}(\epsilon_1^2 - \Delta_1^2)}\right)\tan(k_{Gx}d)$$
$$+\left(\frac{k_{Lx}(\epsilon_1^2 - \Delta_1^2)}{\epsilon_L(\beta\epsilon_1 + k_y\Delta_1)} - \frac{\epsilon_L(\beta\epsilon_1 + k_y\Delta_1)}{k_{Lx}(\epsilon_1^2 - \Delta_1^2)}\right)\tan(k_{Lx}d)$$
$$+\left(\frac{k_{Lx}\epsilon_G}{k_{Gx}\epsilon_L} + \frac{k_{Gx}\epsilon_L}{k_{Lx}\epsilon_G}\right)\tan(k_{Gx}d)\tan(k_{Lx}d) = 2. \tag{6}$$

Eigenmode solutions of the waveguides could be found by using a commercial root solver (*Mathematica* FindRoot), to search for numerical roots k_y of Eq. (6) at a fixed ω. From the imaginary part of complex propagation constant k_y, we

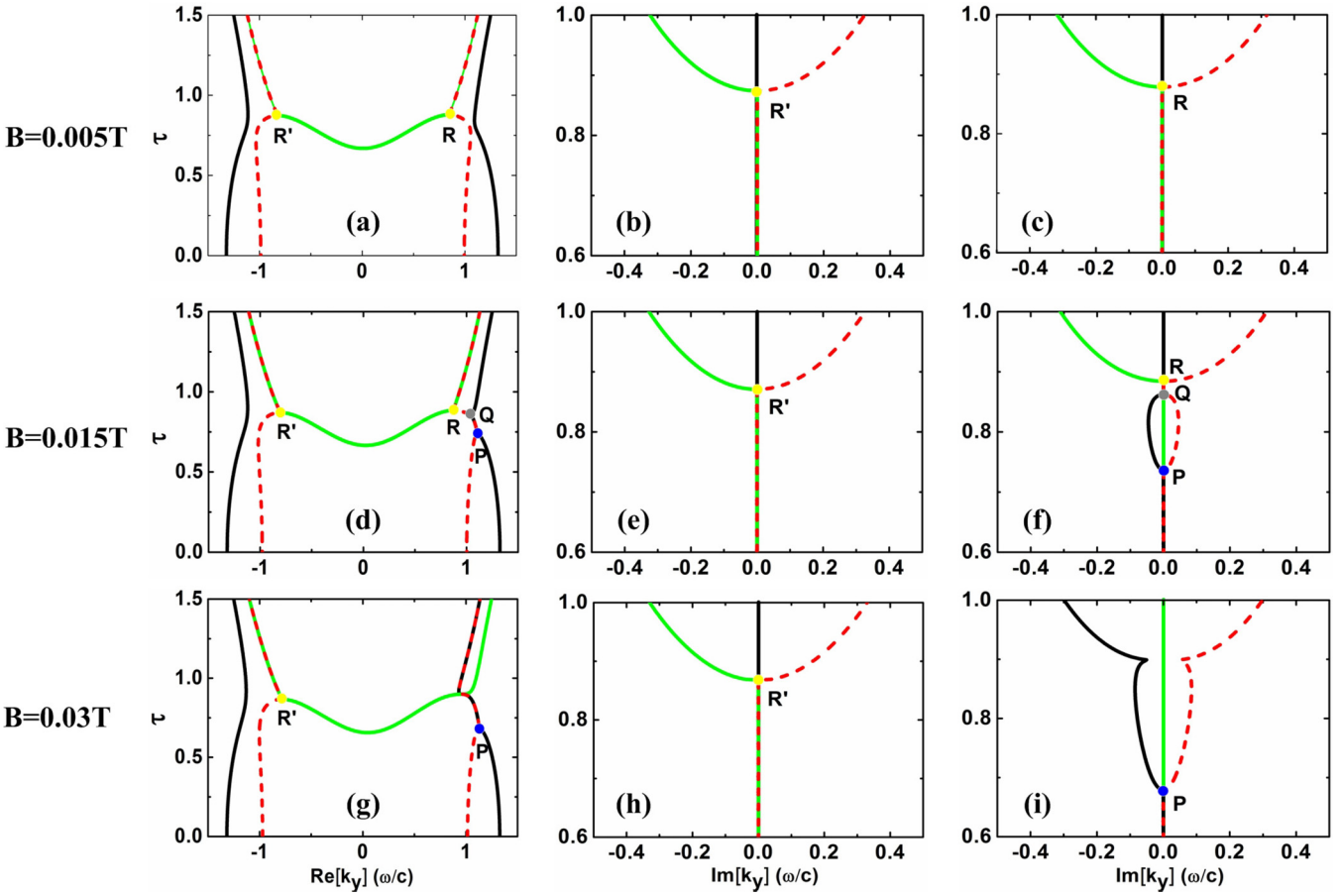

FIG. 2. Loss/gain strength τ versus real parts Re[k_y] and imaginary parts Im[k_y] of the propagation constants, when the magnetic field is present: (a)–(c) $B = 0.005T$, (d)–(f) $B = 0.015T$, and (g)–(i) $B = 0.03T$. Significant nonreciprocity is observed for guided modes, exhibiting a distinct difference in the evolution process of Re[k_y], between negative modes (Re[k_y] < 0) and positive modes (Re[k_y] > 0), shown by the left column, and also of Im[k_y], between negative modes (shown by the middle column) and positive modes [(hown by the right column). Possible EPs occurring in the evolution process of guided modes, i.e., R', R, P, and Q, are marked in respective plots. Other parameters are the same as Fig. 1.

could identify two different phase regimes for the system: $\mathcal{PT}$-symmetric phase with purely real modes, Im[k_y] $= 0$, and $\mathcal{PT}$-broken phase with a pair of complex-conjugate modes, decaying and growing modes, with Im[k_y] $\neq 0$. We emphasize that, due to the presence of an external magnetic field, the linear term of k_y appearing in Eq. (6) breaks the spectral reciprocity (i.e., the left-right symmetry of the dispersion relation), leading to a significant nonreciprocal evolution process on the propagation constants with Re[k_y] > 0 (positive guided modes propagating along the $+y$ direction) and Re[k_y] < 0 (negative guided modes propagating along the $-y$ direction).

III. NONRECIPROCAL EXCEPTIONAL POINTS AND PHASE DIAGRAM

Without loss of generality, here we fix the real part of lossy or gain material with $\epsilon = 2$, and consider a typical kind of SC material, i.e., InSb, in the calculation. The corresponding parameters of InSb at room temperature are taken as $m^* = 0.014m_0$ (m_0 is the free electron mass in vacuum), $\omega_p = 1.26 \times 10^{13}$ Hz, and $\epsilon_\infty = 15.68$. For initial calculations, we neglect the influence of the absorption of SC materials, $\alpha = 0$, and focus on the regime with a given working frequency $\omega = 0.94\omega_p$, and set the thickness of each slab as $d = 0.58 * 2\pi c/\omega$.

Before we investigate the nonreciprocal effect of wave propagation in this $\mathcal{PT}$-symmetric waveguide, below we first look at the normal evolution process of guide modes when the external magnetic field is absent. Figures 1(b) and 1(c) show the real and imaginary parts of propagation constant k_y of guided modes as the loss/gain strength τ increases gradually, where no magnetic field is applied. Two guided modes named as mode 1 and mode 2 are supported at the onset of $\tau = 0$, and they are originally from two coupled surface-plasmon modes occurring near the inner surfaces of the conducting layers, in comparison with the single interface surface-plasmon mode [gray dotted line in Fig. 1(b)]. At small τ, the usual $\mathcal{PT}$ symmetry holds for modes 1 and 2, seen from the purely real k_y. However, another real mode, labeled with mode 3, could be supported when the non-Hermiticity parameter τ turns on. The coupling effect between modes 2 and 3 becomes dominant gradually, tends to pull mode 1 out of the $\mathcal{PT}$-broken phase, and finally modes 2 and 3 merge together, forming a pair of complex modes at the EPs, marked

by R and R' (corresponding to symmetry phase transition for positive and negative guided modes), with complex-conjugate k_y. The original mode symmetry is broken. Notice that the EPs of R and R' occur symmetrically, i.e., the identical τ, for positive ($\mathrm{Re}[k_y] > 0$) and negative ($\mathrm{Re}[k_y] < 0$) guided modes in the absence of an external magnetic field. In this regime, the evolution process of guided modes and phase transition indicates symmetrical and reciprocal.

Next, the external magnetic field is introduced on the two SC slabs, as depicted in Fig. 1(a). To respect the $\mathcal{PT}$ symmetry in the geometric shape, the magnitude of magnetic fields stays uniform, but the applied direction is opposite, i.e., z and $-z$ direction, in the two SC regions. Three different cases are demonstrated in Fig. 2, where the applied magnetic field B varies from $B = 0.005T$, $0.015T$, to $0.03T$. For the small magnetic field, $B = 0.005T$, the original guided modes—either positive or negative modes—and the EPs, R and R', change little, but become substantially asymmetrical and nonreciprocal, although the difference between them is tiny and not obvious, as shown in Figs. 2(a)– 2(c). Interestingly, with increasing the magnetic field, i.e., $B = 0.015T$, seen from Figs. 2(d)– 2(f), the proposed system may display the distinct and significant nonreciprocity on the evolution process in guided modes of different propagation directions. It is found that for the positive guided modes ($\mathrm{Re}[k_y] > 0$), multiple exceptional points, marked by P, Q, and R, occur at $\tau_1 = 0.736$, $\tau_2 = 0.863$, and $\tau_3 = 0.884$, respectively, leading to the emergence of various phase transitions. By looking into the variation of positive modes, modes 1 and 2 merge into a pair of complex modes at the first EP (P), when τ approaches τ_1. The original $\mathcal{PT}$ symmetry is broken. Notably, $\mathcal{PT}$ phase could be restored with a further increase of gain/loss strength, beyond a second EP (Q), and two real modes reappear at $\tau_2 < \tau < \tau_3$. Finally, mode 3 merges with mode 2 into a pair of complex modes at $\tau > \tau_3$, leading to the formation of $\mathcal{PT}$-broken phase beyond a third EP (R). In contrast, for negative modes ($\mathrm{Re}[k_y] < 0$), there is still a relatively small difference during the entire variation process due to the presence of an external magnetic field. When the stronger magnetic field is turned on, i.e., $B = 0.03T$, shown by Figs. 2(g)–2(i), the remarkable nonreciprocity is still present in comparison with positive and negative modes. Meanwhile, regarding the positive modes, the biexceptional points Q and R coalesce with each other and disappear, and only a single EP (P) could be seen. No reentry behavior of $\mathcal{PT}$ symmetry could happen. Again, no distinct variation with negative modes is observed for this case.

It is worthy of noting that the occurrence of coalescence and rebifurcation of EPs shown above is attributed to the competition interacting effect among multiple states, which has also been discussed and analyzed in other multistate systems [19,21,22]. Remarkably, the external magnetic field applied on our proposed $\mathcal{PT}$-symmetric waveguide could effectively tune the interaction among multiple states, but in a nonreciprocal manner, giving rise to the different evolution process between positive and negative guided modes. To show the nonreciprocal effect of the magnetic field clearly, we make a summary on the trajectories of possible EPs and phase diagram for two different propagating directions in the $B - \tau$ space in Fig. 3. When the magnetic field is small, i.e., $B < B_1(\approx 0.0078T)$, the coupling

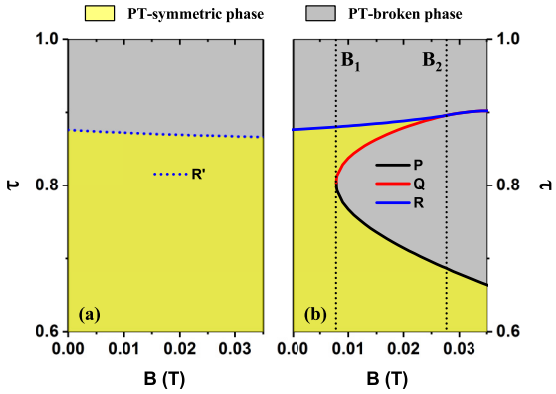

FIG. 3. Trajectories of the exceptional points for negative modes (a) and positive modes (b) in the (B, τ) space: R' (blue dotted line), R (blue solid line), P (black solid line), and Q (red solid line). $\mathcal{PT}$-symmetric and $\mathcal{PT}$-broken phases are indicated by the yellow and gray regions, respectively.

effect between modes 2 and 3 governs the entire system, and leaving mode 1 to be purely real, and only a single phase transition appears at the EP, R or R', for either of the guided modes. The difference in loss/gain strength corresponding to the two EPs is present, but unconspicuous. However, the situation could be changed at higher magnetic field, $B_1 < B < B_2(\approx 0.0275T)$. For positive modes, the attractive interaction between modes 1 and 2 starts to increase gradually, estimated by the emergence of biexceptional points, P and Q, as well as multiple phase transition, i.e., the reentry behavior of $\mathcal{PT}$-symmetric phase. Moreover, as B increases further, $B > B_2$, the interaction between modes 1 and 2 become stronger and dominant, and the EPs, Q and R, tend to moves toward each other, and finally merge together, creating a higher-order singularity. By contrast, there is only a small impact on negative modes as B varies shown in Fig. 3(a). Therefore, in our proposed system, we could possibly achieve significant and distinct nonreciprocity on EPs and phase diagram, even if the external magnetic field is very weak. Very recently, we note that in a wide class of time-periodic systems, other types of EPs with nonreciprocity, i.e., Floquet EPs [31], can occur and give rise to a chiral dynamics, i.e., selection of a different final state in the two directions of rotation starting from the same initial state.

IV. NONRECIPROCAL TRANSPORT PROPERTIES THROUGH FINITE-SIZE $\mathcal{PT}$-SYMMETRIC WAVEGUIDES

As a validation of the $\mathcal{PT}$-symmetric waveguide design based on mode analysis, here we can also directly determine the response of a finite structure illuminated by light using transfer-matrix formalism. Figure 4 presents the transmittance T through a finite waveguide system with its thickness of $w = 0.2 * 2\pi c/\omega$, embedded in a unform surrounding medium $\epsilon_b = 2$, when the external magnetic field is tuned to $B = 0.005T$ and $0.03T$, respectively. The transmittance displays with peaks ($T \sim 1$) within the bands ($\mathcal{PT}$-symmetric phase), while it stays low ($T \sim 0$) or very high ($T > 1$) in the gap region ($\mathcal{PT}$-broken phase). By tuning B slightly, a large variation on transmittance could be observed near the zone

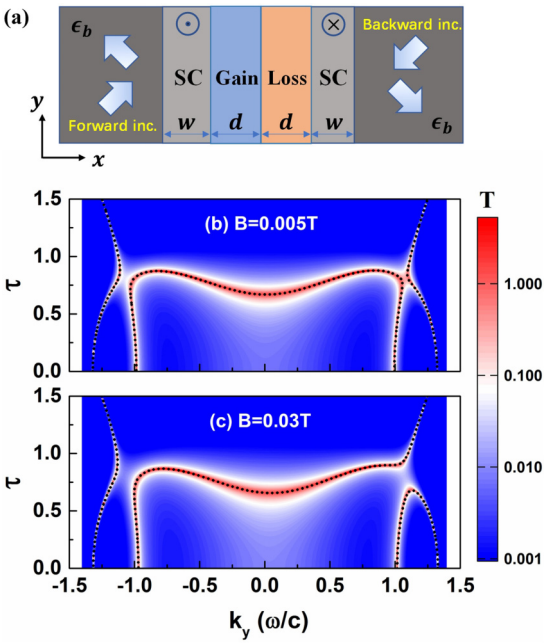

FIG. 4. Nonreciprocal transmittance T of finite-size $\mathcal{PT}$-symmetric slabs embedded in a uniform surrounding medium $\epsilon_b = 2$, when the external magnetic field is applied: (b) $B = 0.005T$ and (c) $B = 0.03T$. We truncate the semi-infinite SC cladding depicted in Fig. 1(a) into two thin slabs with the same thickness $w = 0.2 * 2\pi c/\omega$, and schematically show in (a) such a finite-size system embedded in a uniform surrounding medium $\epsilon_b = 2$. The big arrows guide us to see the incident or reflected beams of light. Other parameters are the same as Fig. 1. For comparison, the associated purely real bands for the infinite systems are also shown with black dotted lines.

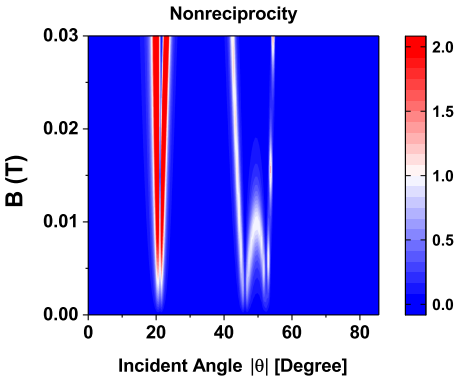

FIG. 5. The differential transmittance versus the magnetic field B and incident angle θ of light, where the amplitude of loss/gain $\tau = 0.8$. Pronounced nonreciprocity in transmission could be seen at some particular incident angles, due to the asymmetrical variation between negative and positive modes.

of EPs owing to the abrupt change of system phase, but only for the forward incidence (incident light propagating along the $+y$ direction). It is also shown that the transmission peaks in each case could map well onto its associated purely real band curves for the infinite systems indicated by black dotted lines. Thus, the nonreciprocal character of guided modes may bring the directional dependence in transmission and result in one-way behavior for this finite-size $\mathcal{PT}$-symmetric system, i.e., complete transmission (or near zero reflection) is allowed for light propagation in one single direction, while in the opposite direction enhanced transmission (or strong reflection) could happen.

For the purpose of clearly demonstrating the sensitivity of nonreciprocity in transmission, which is strongly dependent on magnetic field, we consider a particular case in Fig. 5, where the loss/gain strength is fixed to $\tau = 0.8$. Figure 5 shows the difference in transmittance $|T(+\theta) - T(-\theta)|$ (nonreciprocity) as a function of magnetic field B and the incident angle of light illumination θ. It is found that strong nonreciprocity in transmission (possibly exceeds 1) could be attained at a weak magnetic field, at some particular incident angles, even if for very small magnetic field $B < 0.01T$. Further, we carry out two-dimensional finite-element simulations in Fig. 6 using COMSOL MULTIPHYSICS to confirm the desired results, where the spatial field distribution is calculated at external magnetic field $B = 0.01T$. Figure 6 displays and compares significant nonreciprocity with two examples of different incident angles with $\theta = \pm 20°$ [Figs. 6(a) and 6(b)] and $\theta = \pm 50°$ [Figs. 6(c) and 6(d)]. For the case of forward incidence with $\theta = +20°$ (or $\theta = +50°$), nearly complete transmission is obtained due to the excitation of positive guided modes. In contrast, enhanced transmission ($T > 1$) accompanied simultaneously by strong reflection (backward reflectance $R > 1$) is seen for backward incidence with incident angle $\theta = -20°$ [Fig. 6(b)]. In this sense, the scattering process for backward incidence is superunitary [32], resulted from the breaking of symmetry phase for negative guided modes. However, at incident angle $\theta = -50°$ [Fig. 6(d)], the scattering behavior is subunitary when the system is out of $\mathcal{PT}$-symmetric phase. It is seen that strong reflection ($R < 1$, but close to 1) appears and the transmission is almost completely suppressed ($T \sim 0$). Therefore, by application of asymmetrical phase transitions, we could achieve the pronounced nonreciprocal effect in such a $\mathcal{PT}$-symmetric waveguide, even in the presence of a low-intensity magnetic field.

Until now we have considered lossless SC materials cladding in this waveguide system, where the guided modes in the nonreciprocal zone have purely real wave vectors $\mathrm{Im}[k_y] = 0$ in the forward direction and complex wave vectors $\mathrm{Im}[k_y] \neq 0$ in the backward direction. When the loss is introduced to two sides of the SC layer, guided modes for both directions become complex, but the one-way behavior can still

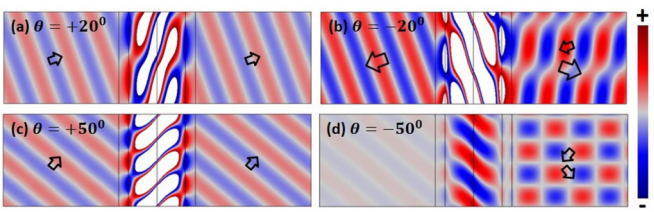

FIG. 6. Field profiles corresponding to two opposite directions of incidence (indicated by arrows) on a finite-size $\mathcal{PT}$-symmetric system, where the magnetic field $B = 0.01T$ and the loss/gain strength $\tau = 0.8$. (a) $\theta = +20°$. (b) $\theta = -20°$. (c) $\theta = +50°$. (d) $\theta = -50°$. Other parameters are the same as Fig. 4.

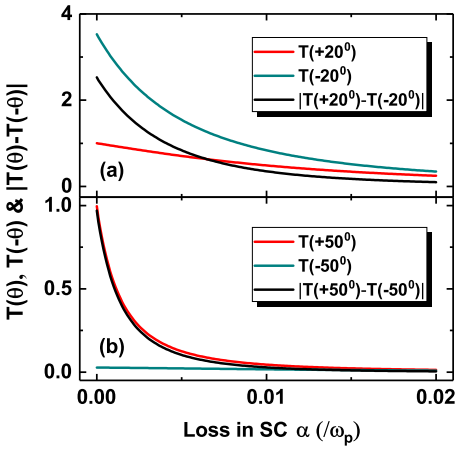

FIG. 7. Nonreciprocal transmittance at an incident angle of (a) $\pm 20^\circ$ and (b) $\pm 50^\circ$, and the corresponding differential transmission, when the loss is introduced identically to the two sides of SC materials. Other parameters are the same as Fig. 6.

be observed for real SC. Finally, we investigate in Fig. 7 the inevitable loss influence in SC materials on the transmission nonreciprocity, when the incident angle $\theta = \pm 20^\circ$ [Fig. 7(a)] and $\theta = \pm 50^\circ$ [Fig. 7(b)] are considered, respectively. Owing to the existence of losses, the transmission for both directions is suppressed to some extent, but is quite robust for moderate loss, i.e., $\alpha < 10^{-2}\omega_p$. The nonreciprocity could still be large, and the difference between forward and backward transmittances can approach 40% or higher, seen from Fig. 7(a).

V. DISCUSSION AND CONCLUSION

For experimental realization of the proposed $\mathcal{PT}$-symmetric system, we may use a typical kind of SC material, such as InSb, in the cladding layers. The external static magnetic field is applied uniformly, but along opposite directions in either side of the cladding regions. Gain and loss are confined to the core domains and implemented by introducing an imaginary part of complex permittivity. A practical way of realizing loss or gain locally and equivalently can be achieved using loss and gain media. Gain media can be commonly achieved by using dye molecules, rare-earth ions, or semiconductor crystals, which can be externally pumped [33]. Here, in comparison with the simulation parameters in the proposed system, we may use Er^{3+}-doped silica [10] as the gain media, while the loss media can be made of silica without dopants. On the other hand, the thickness of gain-loss core layers [and two magnetic SC cladding layers in Fig. 4(a)] is required to be identical to truly realize the structure with $\mathcal{PT}$ symmetry. Slight deviation on the thickness will break the $\mathcal{PT}$ symmetry, leading to the formation of complex guided modes for both directions, but the nonreciprocal transport behavior is still expected to be observed.

In conclusion, we found that a $\mathcal{PT}$-symmetric waveguide sandwiched by an inversely magnetized SC material exhibits significant Lorentz nonreciprocity near the abrupt phase transition due to the emergence and coalescence of multiple exceptional points. In the configuration of $\mathcal{PT}$-symmetric thin films, the nonreciprocity is shown to give rise to one-way light transmission even in the presence of a very weak magnetic field, thereby suggesting an effective method for compact nonreciprocal elements by application of non-Hermitian optical systems.

ACKNOWLEDGMENTS

This work was supported by the Natural Science Foundation of Jiangsu Province (BK20160878), the National Natural Science Foundation of China under Grants No. 11204036 and No. 11374049, the Hong Kong Research Grant Council (15300315, 15301917, AoE/P-02/12), and the Hong Kong Polytechnic University (G-YBPT).

[1] C. M. Bender and S. Boettcher, Phys. Rev. Lett. **80**, 5243 (1998).
[2] C. M. Bender, D. C. Brody, and H. F. Jones, Phys. Rev. Lett. **89**, 270401 (2002).
[3] K. G. Makris, R. El-Ganainy, D. N. Christodoulides, and Z. H. Musslimani, Phys. Rev. Lett. **100**, 103904 (2008).
[4] R. E. Ganainy, K. G. Makris, D. N. Christodoulides, and Z. H. Musslimani, Opt. Lett. **32**, 2632 (2007).
[5] A. Guo, G. J. Salamo, D. Duchesne, R. Morandotti, M. Volatier-Ravat, V. Aimez, G. A. Siviloglou, and D. N. Christodoulides, Phys. Rev. Lett. **103**, 093902 (2009).
[6] A. A. Zyablovsky, A. P. Vinogradov, A. A. Pukhov, A. V. Dorofeenko, and A. A. Lisyansky, Phys. Usp. **57**, 1063 (2014).
[7] S. Longhi, Phys. Rev. Lett. **103**, 123601 (2009).
[8] A. Regensburger, C. Bersch, M.-A. Miri, G. Onishchukov, D. N. Christodoulides, and U. Peschel, Nature (London) **488**, 167 (2012).
[9] Z. Lin, H. Ramezani, T. Eichelkraut, T. Kottos, H. Cao, and D. N. Christodoulides, Phys. Rev. Lett. **106**, 213901 (2011).
[10] B. Peng, S. K. Özdemir, F. Lei, F. Monifi, M. Gianfreda, G. L. Long, S. Fan, F. Nori, C. M. Bender, and L. Yang, Nat. Phys. **10**, 394 (2014).
[11] L. Feng, Y. Xu, W. S. Fegadolli, M. Lu, J. E. B. Oliveira, V. R. Almeida, Y. Chen, and A. Scherer, Nat. Mater. **12**, 108 (2013).
[12] X. Zhu, L. Feng, P. Zhang, X. Yin, and X. Zhang, Opt. Lett. **38**, 2821 (2013).
[13] E. Yang, Y. Lu, Y. Wang, Y. Dai, and P. Wang, Opt. Express **24**, 14311 (2016).
[14] S. Longhi, Phys. Rev. A **82**, 031801(R) (2010).
[15] Y. D. Chong, L. Ge, and A. D. Stone, Phys. Rev. Lett. **106**, 093902 (2011).
[16] Z. Lin, A. Pick, M. Lončar, and A. W. Rodriguez, Phys. Rev. Lett. **117**, 107402 (2016).
[17] J. Wiersig, Phys. Rev. A **93**, 033809 (2016).
[18] H. Alaeian and J. A. Dionne, Phys. Rev. B **89**, 075136 (2014).
[19] K. Ding, Z. Q. Zhang, and C. T. Chan, Phys. Rev. B **92**, 235310 (2015).

[20] B. Zhen, C. W. Hsu, Y. Igarashi, L. Lu, I. Kaminer, A. Pick, S.-L. Chua, J. D. Joannopoulos, and M. Soljačić, Nature (London) **525**, 354 (2015).
[21] K. Ding, G. Ma, M. Xiao, Z. Q. Zhang, and C. T. Chan, Phys. Rev. X **6**, 021007 (2016).
[22] J. Wang, H. Y. Dong, R. P. H. Wu, T. C. Mok, and K. H. Fung, Opt. Lett. **42**, 535 (2017).
[23] S. N. Ghosh and Y. D. Chong, Sci. Rep. **6**, 19837 (2016).
[24] H. Cartarius, J. Main, and G. Wunner, Phys. Rev. Lett. **99**, 173003 (2007).
[25] C. Huang, F. Ye, Y. V. Kartashov, B. A. Malomed, and X. Chen, Opt. Lett. **39**, 5443 (2014).
[26] S.-Y. Lee, J.-W. Ryu, S. W. Kim, and Y. Chung, Phys. Rev. A **85**, 064103 (2012).
[27] W. D. Heiss, J. Phys. A: Math. Theor. **41**, 244010 (2008).
[28] G. Demange and E.-M. Graefe, J. Phys. A: Math. Theor. **45**, 025303 (2012).
[29] Z. Yu, G. Veronis, Z. Wang, and S. Fan, Phys. Rev. Lett. **100**, 023902 (2008).
[30] B. Hu, Q. J. Wang, and Y. Zhang, Opt. Lett. **37**, 1895 (2012).
[31] S. Longhi, J. Phys. A: Math. Theor. **50**, 505201 (2017).
[32] L. Ge, Y. D. Chong, and A. D. Stone, Phys. Rev. A **85**, 023802 (2012).
[33] A. Manjavacas, ACS Photonics **3**, 1301 (2016).